IEEE Robotics and Automation Letters (RAL) paper presented at the
2020 IEEE/RSJ International Conference on Intelligent Robots and Systems (IROS)
October 25-29, 2020, Las Vegas, NV, USA (Virtual)

Piezoelectric grippers for mobile micromanipulation

Tristan Abondance[1,2], Kaushik Jayaram[3], Noah T. Jafferis[1], Jennifer Shum[1], and Robert J. Wood[1]

***Abstract*— The ability to efficiently and precisely manipulate objects in inaccessible environments is becoming an essential requirement for many applications of mobile robots, particularly at small sizes. Here, we propose and implement a mobile micromanipulation solution using a piezoelectric microgripper integrated into a dexterous robot, HAMR (the Harvard Ambulatory MicroRobot), that has a size of approximately $4.5\,\mathrm{cm}$ by $4\,\mathrm{cm}$ by $2.3\,\mathrm{cm}$ and a maximum payload of approximately $3\,\mathrm{g}$. Our $100\,\mathrm{mg}$ miniature gripper is composed of recurve piezoelectric actuators that produce parallel jaw motions (stroke of $236 \pm 32\,\mu\mathrm{m}$ at $200\,\mathrm{V}$) while providing high gripping forces (blocked force of $0.575\,\mathrm{N}$ at $200\,\mathrm{V}$), making it effective for micromanipulation applications with tiny objects. Using this gripper, we successfully demonstrated a grasping and lifting task with an object of $1.3\,\mathrm{g}$ and thickness of $250\,\mu\mathrm{m}$ at an operating voltage of $100\,\mathrm{V}$. Finally, by taking advantage of the locomotion capabilities of HAMR, we demonstrate mobile manipulation by changing the position and orientation of small objects weighing up to $2.8\,\mathrm{g}$ controlled by the movement of the robot. We expect that the addition of this novel manipulation capability will increase the effectiveness of such miniature robots for accomplishing real-world tasks.**

***Index Terms*— Grippers and Other End-Effectors, Micro/Nano Robot, Mobile Manipulation, Grasping, Piezoelectric actuators.**

I. INTRODUCTION

Bio-inspired robots at the insect scale can reach confined environments and places inaccessible to humans [1] and therefore represent a great potential for mobile micromanipulation [2]. Their capabilities are evolving: microrobots have demonstrated the ability to fly [3], perch [4], swim [5], move on vertical or inverted surfaces [6], crawl on rough terrain [7], and even walk on water [8]. However, most research so far has focused more on the mobility [9] and control [10] of these robots, and less on their real world functionalities. For example, few of these small robots are able to perform complex tasks such as picking up objects and moving them to a desired location [11]. Adding such a capability could open up new possibilities such as depositing, collecting, and returning materials in inaccessible or remote environments [12]. In addition to object manipulation, microgrippers are expected to be useful as components of more complex mechanical mechanisms, such as clutches for devices that amplify the stroke of a primary actuator for frequency-leveraging [13].

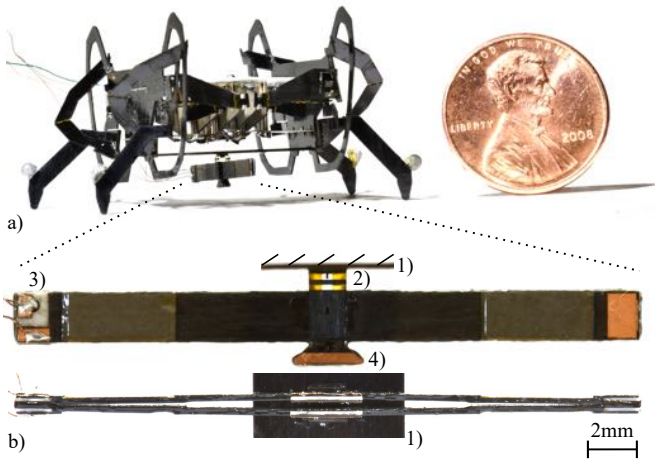

Fig. 1. (a) The gripper mounted under HAMR. (b) Close up side and bottom views of the gripper: (1) beam mounted on the ventral side of the HAMR; (2) gripper support composed of a kapton hinge; (3) electrical connections; and (4) gripper jaw.

Developing a microgripper that has a mass, volume, and power consumption sufficiently low to be incorporated into miniature robots represents a significant challenge. In addition, such a gripper must be able to provide adequate force to carry objects (up to the maximum payload of the robot) while the robot is moving, and be adaptable to grasp objects of various shapes, sizes, and weights.

In this manuscript, we address these challenges by designing (Sec. II), and fabricating (Sec. III) a low mass ($0.1\,\mathrm{g}$), high force (up to $0.575\,\mathrm{N}$) piezoelectric microgripper (Fig. 1). We modeled the free deflection and blocked force for the proposed gripper designs (Sec. IV) and used the model to guide our designs. We then characterized the gripper performance by quantifying the above metrics in Sec. V. We integrated this microgripper into our insect scale quadrupedal robot, the Harvard Ambulatory MicroRobot (HAMR) [14] and demonstrated that it could be used for multiple mobile micromanipulation applications (Sec. VI) including object lifting, relocation and reorientation.

II. DESIGN

A variety of microgripper designs [15] and their corresponding actuation technologies [16] have been demonstrated

This work is partially funded by the Wyss Institute for Biologically Inspired Engineering, the DARPA SHort Range Independent Microrobotic Platforms (#HR001119C0044, to R.J.W.) and the Department of Defense (DoD) through the National Defense Science & Engineering Graduate (NDSEG) Fellowship Program (to J.S.). The views, opinions and/or findings expressed are those of the author and should not be interpreted as representing the official views or policies of the Department of Defense or the U.S. Government. Distribution Statement "A" (Approved for Public Release, Distribution Unlimited).

[1]Harvard Microbotics Lab, School of Engineering and Applied Sciences, Harvard University and Wyss Institute of Biological Engineering, rjwood@seas.harvard.edu

[2]Department of Microengineering, Ecole Polytechnique Fédérale de Lausanne, tristan.abondance@alumni.epfl.ch

[3]Department of Mechanical Engineering, University of Colorado Boulder, kaushik.jayaram@colorado.edu

in literature. A review of recent research has indicated that the key requirements for an optimal microgripper design were (1) high gripping force and stroke output, while minimizing the weight and volume [17], and (2) high grasping accuracy generated by the parallel motion of the jaws [18].

A. Laminated piezoelectric actuators

Given these considerations, we chose piezoelectric actuators as the most promising option for gripping mechanisms due to their high force density [17]. Additionally, since they are already used as the primary actuation technology for numerous micorobots, including the RoboBee [3] and HAMR [19], the relatively high voltages (approximately 100 to 200 V) required to operate them are already available in such systems, and their onboard control systems can therefore be easily modified to drive the gripper.

B. Recurve architecture

Having determined our actuation technology, we chose a dual recurve actuator architecture [20] for our piezoelectric microgripper due to its potential for maximizing specific work output ($output\ stroke \times force/weight$) [21] while maintaining a parallel jaw configuration [22] (Fig. 2).

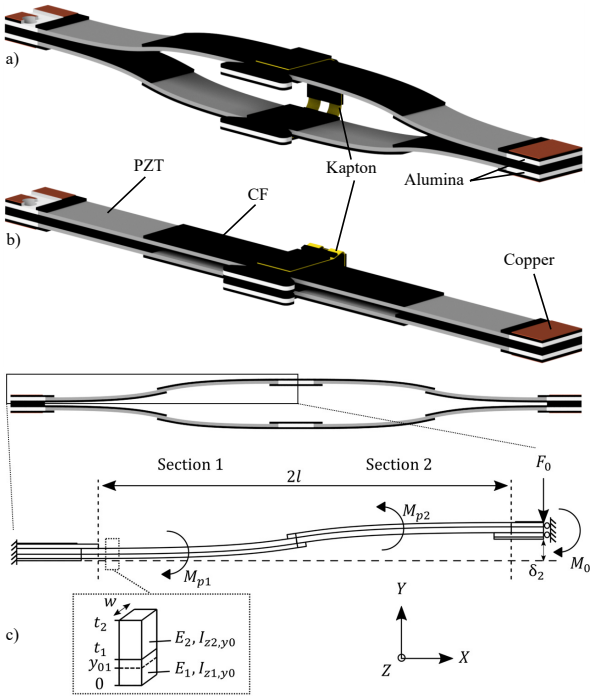

Fig. 2. Operation of the proposed microgripper: (a) gripper open; (b) gripper closed. Gripper stroke is exaggerated for illustrative purposes. (c) Notation of forces and moments applied on an activated single recurve element with an active part of length 2l.

A fundamental recurve element is a cantilever beam composed of one or more active layers and passive layers. These layers are configured such that when actuated, the first part of the beam has a positive curvature and the second has a negative curvature as shown in Fig. 2. Since the two parts of the beam are of equal length, and their curvatures are equal in magnitude but opposite in sign, we obtain free deflection vertically at the end of the beam without rotation. However, if an external force is applied at the end such as during manipulation, the gripper ends are no longer constrained to move parallel to each other. To resolve this, we combined four recurve elements (two in series and two in parallel) to form an array architecture as described in [20] (Fig. 2). Further, we chose a unimorph (one active layer and one passive layer) configuration for the recurve element because this nominally avoids tensile strain in the active layer (which contracts with applied electric field) and therefore, is beneficial for the longevity of the microgripper [23].

C. Unactuated configuration

Another design consideration for our gripper is the operating mode – here, we choose a normally closed configuration. To grasp an object, the gripper is first actuated to open the jaws, then deactivated to close the jaws. This mode uses less energy as most of the time the gripper will be closed – an important criterion for untethered mobile robots. However, the closing force depends on the stiffness of the actuator and the size of the object, i.e., larger objects passively cause greater elastic strain of the actuator and therefore greater gripping force. Thus for applications such as handling of delicate objects that require a low gripping force, the output force can be modulated by partially actuating the gripper jaws.

An advantage of this gripper design is it's adaptable gripping range. The distance between the two jaws can be adjusted according to the thickness of the CF layer used to bond the upper and lower laminates of the gripper together.

III. FABRICATION

A. Material selection

Lead zirconium titanate (PZT, Navy Type V) is used for the active layer as it has a high piezoelectric force coefficient and is easy to machine using bulk micromachining techniques. For the passive layer, we used a carbon fiber composite (CF) for both for its mechanical properties (high Young's modulus E_1 of 340 GPa and a low density of $1.6\,\mathrm{g/cm^3}$), and to facilitate the fabrication process – the resin in the uncured CF provides a strong mechanical bond upon lamination, and the carbon fibers provide electrical conductivity to the PZT electrodes (Fig. 2). Alumina is added to the end of the actuator as rigid non-conductive extensions of the PZT-CF part. This was sized to be large enough to facilitate actuator manipulation and to be used as a support for the external electrical connections. A thin sheet of copper is bonded on top of the alumina parts, to allow electrical wiring via soldering.

The thickness of the different materials was restricted by their off-the-shelf availability. The PZT, being a brittle ceramic, was difficult to find in thin sheets at reasonable costs, so a 135 µm sheet was used. To optimize bonding, we used alumina of similar thickness (127 µm). We used two CF layers of 50 µm each to bring the overall CF thickness to 100 µm. The other actuator dimensions were free to choose and depended on the desired performance.

B. Laminate fabrication procedure

Manufacturing of the microgrippers (Fig. 3) is based on the lamination process developed in [24] and is briefly described below. Pieces of PZT and alumina are cut to the desired shape using a DPSS laser (Oxford Lasers E Series). They are placed on a tacky layer (Gelpak 4) to hold them in place, and within a custom fiberglass (FR-4) jig to align the components. Pre-patterned layers of CF and copper (for electrodes) are then added into the pin-aligned jig. This first stack of materials is placed in a heat press (Carver Auto Series NE) for a brief tacking so that the resin in the CF flows and the PZT and alumina parts are fixed to the CF layer. Then the Gelpak layer is removed and replaced by two additional layers of CF. This laminate (one half of the gripper) is placed for two hours in the heat press at a temperature of $180\,^{\circ}\mathrm{C}$ under a pressure of $30\,\mathrm{PSI}$ for the resin in the CF to be completely cured. After this, the top and bottom copies of the gripper are bonded together by adding one layer of CF in between and placing the stack in the heat press for a second cure process under the same conditions. The laminate is removed from the press and laser cut to release the complete grippers. After cleaning thoroughly with isopropyl alcohol, cyanoacrylate glue is manually applied to the edges of the actuators to prevent shorting. Finally, the center layer of the gripper is connected to the copper layer using conductive epoxy through holes in the alumina and wires are soldered to complete the electrical connections needed for actuation (Fig. 1b).

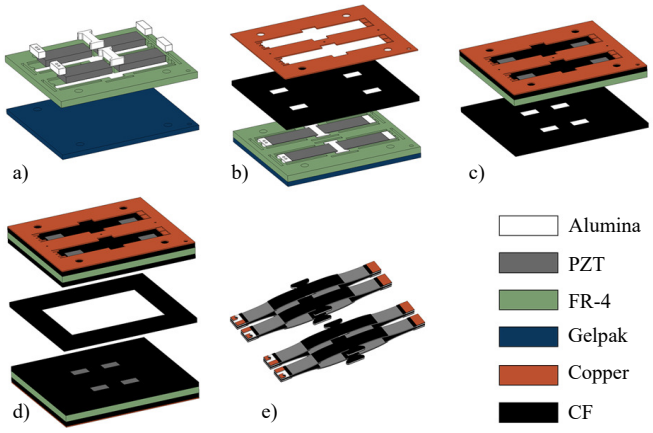

Fig. 3. Process steps for manufacturing four grippers. a) Laser-cut PZT and alumina pieces are manually placed into a laser-cut FR4 jig mounted on gelpak. b) Two layers of CF and one layer of copper are "tacked" onto the PZT and alumina. c) The gelpak is removed and replaced with two layers of CF, and a full cure is performed. d) Two copies of (c) are bonded together by adding one layer of CF in between and using a heat press. e) Final grippers after release cut with laser.

IV. MODELING

In order to size our grippers for various applications, we developed an analytical model for predicting the performance (stroke, force) based on the theory of recurve actuators [20][21]. In this model, only the active part defined in Fig. 2c, composed of layers of CF and PZT, is evaluated. Because these two materials have different thicknesses and moduli, the neutral axis is not located in the center of the beam but shifted out of the PZT, as desired for maximizing output energy. The location of the neutral axis y_0 is computed by applying the equilibrium conditions on a section of the beam composed of materials with Young's modulus E_i, and a radius of curvature ρ as:

$$\sum F_x = \iint \sigma_x(x,y)\,dy\,dz = \sum_i \iint E_i \frac{y-y_0}{\rho}\,dy\,dz = 0 \tag{1}$$

$$y_0 = \frac{\sum_i \iint E_i y\,dy\,dz}{\sum_i \iint E_i\,dy\,dz} \tag{2}$$

Using equation (2), the neutral axis y_{0_1} is computed for the first section of the beam as:

$$y_{0_1} = \frac{\int_0^{t_1}\int_0^{w} E_1 y\,dz\,dy + \int_{t_1}^{t_2}\int_0^{w} E_2 y\,dz\,dy}{\int_0^{t_1}\int_0^{w} E_1\,dz\,dy + \int_{t_1}^{t_2}\int_0^{w} E_2\,dz\,dy} \tag{3}$$

The second moment of area of the CF layer, I_{z_1,y_0}, and of the PZT layer, I_{z_2,y_0}, in the first section are determined with respect to the neutral axis as:

$$I_{z_1,y_0} = \int_0^{t_1}\int_0^{w} (y-y_0)^2\,dz\,dy \tag{4}$$

$$I_{z_2,y_0} = \int_{t_1}^{t_2}\int_0^{w} (y-y_0)^2\,dz\,dy \tag{5}$$

The effect of the activated piezoelectric layer on this recurve actuator is modeled by two moments M_{P_1} and M_{P_2} applied in sections one and two, respectively, as shown in Fig. 2c. The internal moment of a piezoelectric beam activated by an electric field $\mathcal{E}_2$ was defined by Crawley at al., [25] as:

$$M_p = \int\int \sigma_x(x,y)\,dy\,dz = \int_{t_1}^{t_2}\int_0^{w} f_{31}\mathcal{E}_2(y-y_0)\,dz\,dy \tag{6}$$

where f_{31} is the stress generated in the PZT per applied electric field. The PZT properties vary with strain, so two different values of f_{31} were used for the free deflection and blocked force measurement according to Jafferis et al. [24], (f_{31} also varies with electric field, but here we use only the high-field values from [24]). The PZT Young's modulus E_2 increases when it is compressed, but for simplicity we used the zero-strain value of $40\,\mathrm{GPa}$ for both our blocked force and free deflection calculations. This is expected to be the cause of the reduced slope of the free deflection data above approximately $100\,\mathrm{V}$ [24]. The symmetry of the recurve means that the same moment is applied in the second section of the recurve actuator, which gives $-M_{P_1} = M_{P_2} = M_P$.

To simplify the analysis hereafter, we make the following assumptions. First, we neglect the changes in the modulus of the piezoelectric material as a function of strain and voltage. Second, we assume that the beam is in pure bending, meaning that transverse shear stresses are negligible. Furthermore, we assume that actuator mass is much smaller than the blocked force, and therefore, the effect of gravity is neglected. Finally, we neglect forces along the x-axis because

the gripper is mounted at its center and its two ends are free to move.

Now, applying the loading condition represented in Fig. 2c, we can determine the moment along the actuator length as:

$$M(x) = \begin{cases} M_P + M_0 - F_0(2l - x) & 0 \leq x \leq l \\ -M_P + M_0 - F_0(2l - x) & l \leq x \leq 2l \end{cases} \quad (7)$$

By double integrating the moment, divided by the composite stiffness (D), we obtain deflection (δ) as:

$$\delta(x) = \int\int \frac{M(x)}{D} dx dx \quad (8)$$

$$\delta(x) = \begin{cases} \frac{1}{D}(\frac{M_P x^2}{2} + \frac{M_0 x^2}{2} - \frac{F_0(2l-x)^3}{6} - \\ 2F_0 l^2 x + \frac{8F_0 l^3}{6}) & 0 \leq x \leq l \\ \frac{1}{D}(-\frac{M_P x^2}{2} + \frac{M_0 x^2}{2} - \frac{F_0(2l-x)^3}{6} + \\ 2M_P l x - 2F_0 l^2 x - M_P l^2 + \frac{8F_0 l^3}{6}) & l \leq x \leq 2l \end{cases} \quad (9)$$

where,

$$D = E_1 I_{z_1,y_0} + E_2 I_{z_2,y_0} \quad (10)$$

Thus, the free deflection (δ_{free}) of the recurve actuator is determined by setting the force at the distal end to zero as:

$$\delta_{free} = \delta(x = 2l | F_0 = 0) = \frac{M_P l^2}{D} \quad (11)$$

The blocked force (F_{Block}) is obtained when the total deflection of the beam is equal to zero as:

$$\delta(x = 2l) = 0 \iff F_{Block} = \frac{3M_P}{2l} \quad (12)$$

A. Sizing of the microgripper

The above analysis is representative for one recurve element only. However, our proposed gripper (Fig. 2) is composed of two elements in series and two in parallel, therefore the free deflection and blocked force of the whole system are each twice the value computed in equations (11) and (12), respectively [22].

We designed the gripper to have a free deflection greater than $250\,\mu m$. Based on the model estimate from equation (11), and given the material thicknesses specified earlier, the minimum length of the active PZT required in each recurve element was determined to be $9.11\,mm$. Thus, we set the PZT length l to $10\,mm$, and for ease of fabrication and gripper integrity, we added $0.8\,mm$ of CF overlap (Fig. 2), which reduced the active PZT length l to $9.2\,mm$. On a related note, we choose a single CF spacer layer ($50\,\mu m$) and thus had a theoretical gripping range of $50\,\mu m$ to $300\,\mu m$. The spacing layer of CF can be varied depending on specific application to achieve the required gripping range.

Further, we wanted to have a gripper that could carry the entire payload of HAMR which is approximately $3\,g$ [26]. Assuming a factor of safety of approximately two, a minimum coefficient of friction of 0.1, and operation at $200\,V$, the minimum required active PZT element width from equation (12) was determined to be approximately $2\,mm$.

To enable the gripper to be conveniently used on many microrobots and increase the ease of manipulation, we created two jaws by extending the rigid alumina, which is present at the interface between the two recurve elements, as shown in Fig. 2. Thus, the completed grippers had a mass of $100\,mg$ and a volume of $24.5\,mm \times 3\,mm \times 0.81\,mm$, well within our desired weight and size constraints.

V. CHARACTERIZATION & PERFORMANCE

We characterized the performance of the fabricated grippers by quantifying free deflection and blocked force as a function of voltage ranging from $50\,V$ to $200\,V$. Six grippers from two different fabrication batches were tested for at least five cycles to minimize the measurement error. As the grippers N1, N2 and N4 failed after high number of cycles at high voltage, we restricted this voltage to $100\,V$ for the other grippers. Before any testing, the actuators were first repoled to avoid any depolarization resulting from the fabrication process.

We observed that the initial gap between the jaws was greater than the $50\,\mu m$ spacer layer thickness, and varied (from $100\,\mu m$ to $150\,\mu m$) across the actuators. This larger gap is due to the difference in the coefficients of thermal expansion between the PZT and CF layers, which causes deformation of the actuators during cure. We suspect that the variation between actuators is due to variation in layer thicknesses and position of the actuator within the layup. While this is not expected to effect the free deflection or blocked force of the gripper, it will affect the size of the object that can be manipulated.

A. Free deflection

In order to quantify the free deflection at the tip of the gripper, we used a high-zoom inspection camera (PixeLINK PL-B741F) mounted on an adjustable micropositioning stages.

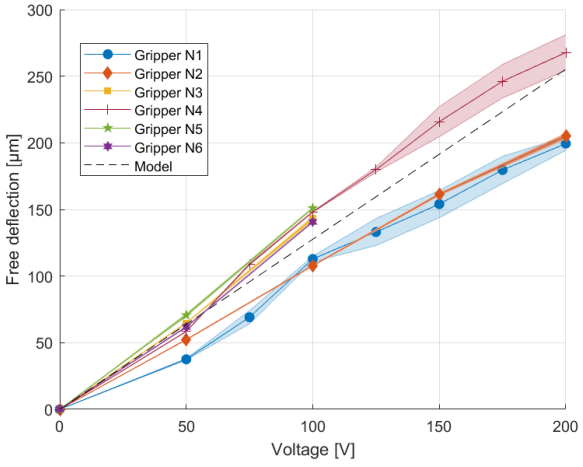

Fig. 4. Free deflection measurements for six grippers, compared to model predictions. Each data point represents the average over a number of at least five deflection cycles. For gripper N1, the camera image scale was estimated from the length of known features on the gripper, while for grippers N2 to N6, it was determined from the camera characteristics ($1.5\,\mu m$/pixel). The shaded regions represent the ± 1 S.D. for gripper N1, N2 and N4. For the other grippers the S.D. is too small to be visible in the plot ($<2\,\mu m$).

The gripper was securely mounted on an acrylic plate at the bottom alumina piece in the view of the camera. Once the voltage was applied as described above, gripper deflection data was extracted from the calibrated videos using a commercial tracking software (Tracker). The maximum deflection was defined as the distance between the starting position and the average peak deflection.

The reference value was determined from our model equation (11) with moments computed with PZT coefficient f_{31} value of $30\,\mathrm{Pa\,m/V}$ according to the free deflection model [24]. We found that free deflection increased linearly as a function of voltage and ranged from $0\,\mu\mathrm{m}$ at $0\,\mathrm{V}$ to $236 \pm 32\,\mu\mathrm{m}$ at $200\,\mathrm{V}$ (Fig. 4). Our measured data was close to the model predictions, with an average error of approximately $23\,\%$ lower, $17\,\%$ lower, $7\,\%$ higher, $9\,\%$ higher, $15\,\%$ higher and $4\,\%$ higher for grippers N1 to N6, respectively. A maximum deflection of $268\,\mu\mathrm{m}$ at $200\,\mathrm{V}$ was obtained compared to $255\,\mu\mathrm{m}$ predicted by our model. Possible sources of the discrepancies between the model and experiments include variations in CF layer thickness and modulus and fabrication conditions across grippers.

B. Blocked force

To measure the blocked force, a high resolution force sensor (ATI Nano 17) was added to the deflection measurement setup. It was mounted to a linear stage to be positioned so that it exerts a slight pressure on the actuator at its initial position to ensure that it remains in contact with the actuator during experiments. The camera is used to adjust the sensor position on the actuator. Force measurements were performed under the same conditions and with the same grippers used for deflection measurement. Sensor data is acquired at a sampling frequency of $100\,\mathrm{Hz}$. A low pass filter with a pass-band frequency of $1\,\mathrm{Hz}$ was applied to attenuate noise signals from the force sensor. The force is measured by extracting the peak values from the filtered signal.

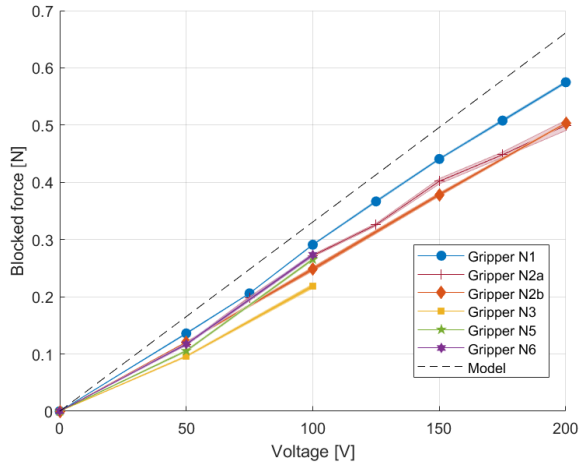

Fig. 5. Blocked force measurements for six grippers, compared to model predictions. Gripper N2a and N2b are the same gripper, but the force is measured at slightly different positions within the rigid output. The standard deviation is too small to be visible in the plot ($<9\,\mathrm{mN}$).

The reference value was determined from our model equation (12) with moments computed with PZT coefficient f_{31} value of $25\,\mathrm{Pa\,m/V}$ according to the zero strain model [24]. We found that blocked force increased linearly as a function of voltage and ranged from $0\,\mathrm{N}$ at $0\,\mathrm{V}$ to $0.575\,\mathrm{N}$ at $200\,\mathrm{V}$ (Fig. 5). These results show that our model over estimates the gripper blocked force with an average error of approximately $13.5\,\%$, $22\,\%$, $25\,\%$, $38\,\%$, $28\,\%$ and $23\,\%$ for grippers N1, N2a, N2b, N3, N5 and N6 respectively. As with the free deflection, one possible cause of this discrepancy is the variation of the CF thickness and modulus (e.g., note that the gripper with the highest deflection has the lowest force). Additionally, the lower measured forces could be due to imperfect bonding and/or parasitic compliance in the gripper or measurement setup. However, it should be noted that the experimentally measured forces were extremely repeatable with standard deviation for each measurement set being less than $1\,\%$ on average for all measurements.

VI. MOBILE MICROMANIPULATION

One of the smallest [19] and yet highly articulated insect-scale quadrupedal legged robots is the Harvard Ambulatory MicroRobot, HAMR [14], shown in Fig. 1 and 6. The diverse capabilities [6][7][8][10] of HAMR make it an ideal platform for exploring mobile micromanipulation. As a first step towards exploring this novel capability, we mounted our piezoelectric grippers onto HAMR-VI ($4.5\,\mathrm{cm}$ in length, $1.41\,\mathrm{g}$ in weight, [26]) as shown in Fig. 6. For this purpose, we designed a custom adapter that securely attaches the microgripper to HAMR, while allowing both its jaws to move freely. The adapter is a one degree of freedom laminate hinge mechanism that connects the central alumina section on each side of the gripper (Fig. 2) to a stiff beam mounted on the ventral side of HAMR. We performed all manipulation tests using the gripper on the robot at a voltage of $100\,\mathrm{V}$ while the robot actuator were driven with a peak voltage of $200\,\mathrm{V}$.

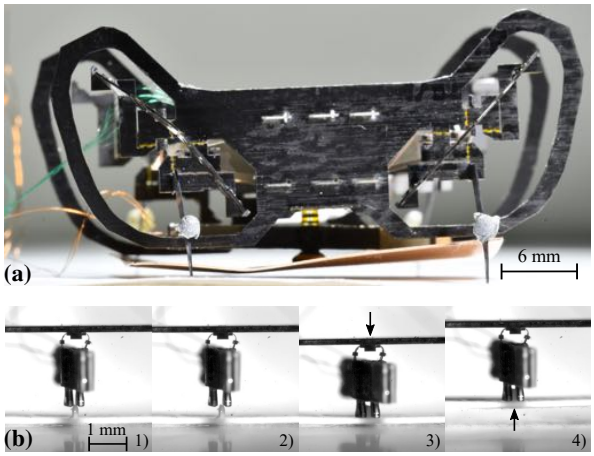

Fig. 6. (a) Gripper on HAMR holding an object of $1.3\,\mathrm{g}$. (b) In (1) the gripper is inactive (closed), and above the object to be gripped. In (2), the gripper is opened. In (3), HAMR lowers, so the gripper moves down over the object to be gripped. In (4), the gripper has been closed, and HAMR has moved up again, lifting the object.

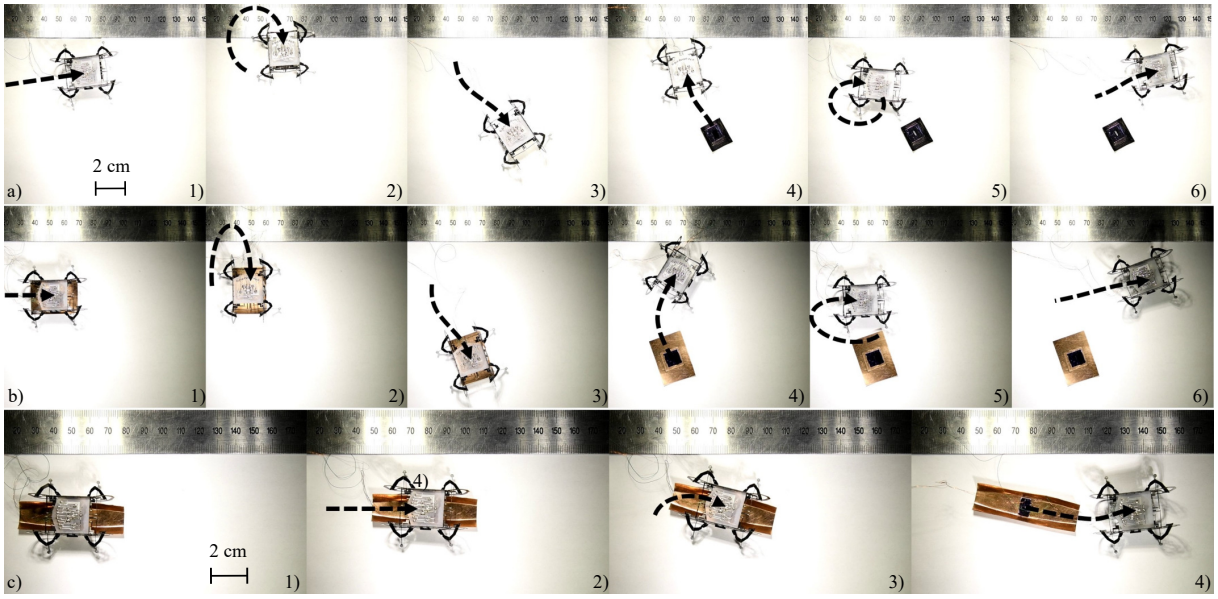

Fig. 7. Manipulation of three objects of different weights (a: 0.5 g, b: 1.3 g, and c: 2.8 g). In (a), the object is carried, while in (b) and (c), it is dragged. The same movement sequences are performed in (a) and (b): (1) HAMR picks up an object below it and moves forward, (2) rotates clockwise, (3) moves forward and drops the object, (4) moves backward, (5) rotates counterclockwise, and (6) moves forward. For (c), the weight was heavier, so HAMR was struggling to move properly and therefore only (1) picks up the object below it, (2) moves forwards, (3) rotates clockwise and drops the object, and (4) moves forward.

When mounted on HAMR, the clearance under the gripper is less than $1.5\,\mathrm{mm}$, so only thin objects could be picked up. We fabricated custom objects using thin layers of phosphor bronze, at various sizes to provide different weights. A thin 3D printed plastic handle was bonded of the bronze layer to provide a tab for ease of gripping. In order to perform the manipulation tests, we manually placed the object under the jaws of the gripper. We then actuated the gripper to open the jaws, commanded the robot to lower, closed the gripper, and then commanded the robot to raise up. The robot could lift objects up to $1.3\,\mathrm{g}$ with a tip thickness of $250\,\mu\mathrm{m}$, as shown in Fig. 6a. The gripper seemed to benefit from the flexible hinge in the adapter which compensated for small misalignment with the object. The gripper-equipped robot was able to carry an object of $0.5\,\mathrm{g}$ while moving. Although the robot could lift heavier objects, ground interactions due to the compliance of the robot limited its carrying performance. However, the robot was able to drag objects up to $2.8\,\mathrm{g}$ on the ground (the maximum payload capacity of the robot was around $3\,\mathrm{g}$). Using this setup, we are beginning to explore basic mobile manipulation operations such as re-positioning and re-orientation objects as shown in Fig. 7.

Further, we note that the gripper itself can hold a maximum weight of approximately $4.1\,\mathrm{g}$ (gripping an approximately $260\,\mu\mathrm{m}$ thick paper tab attached to a weight) at only $100\,\mathrm{V}$ as shown in Fig. 8, which already exceeds HAMR's payload.

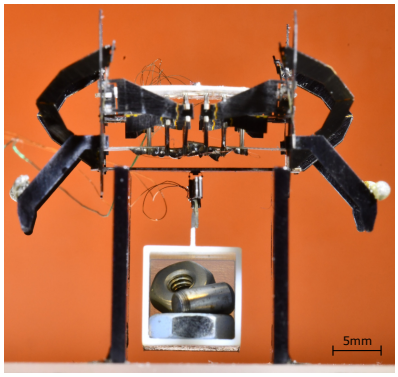

Fig. 8. A structure supports the robot in order to test the maximum weight that the gripper can hold. By driving the gripper at $100\,\mathrm{V}$ to open the jaws, it can hold an object of $4.1\,\mathrm{g}$ with a thickness of $260\,\mu\mathrm{m}$.

VII. DISCUSSION & FUTURE WORK

This paper describes the design and manufacturing of a mobile micromanipulator for use in insect-scale robots. By leveraging a recurve architecture, we built a gripper that provided a gripping force of $0.575\,\mathrm{N}$ with dimensions of $24.5\,\mathrm{mm} \times 3\,\mathrm{mm} \times 0.81\,\mathrm{mm}$ and a weight of $100\,\mathrm{mg}$. The best performing gripper had a maximum gripping stroke of $268\,\mu\mathrm{m}$ and was able to carry objects of varying thicknesses from 100 to $368\,\mu\mathrm{m}$. We summarize the capabilities of our gripper in Tab. I and compare it against others published in recent literature of similar sizes. Tab. I indicates that our microgripper has similar performance to existing designs in terms of force and deflection, but is significantly smaller in mass and/or volume. Related, it is also important to highlight that our prototypes demonstrate a specific work nearly eight times higher compared to other microgrippers that include actuation mechanisms [27][28].

We also showed that our gripper could be easily integrated on an insect scale microrobot. We demonstrated that while mounted on HAMR, we were able to pick up objects up to

TABLE I

CHARACTERISTICS OF DIFFERENT MICROGRIPPERS

Ref.	**Dimensions** $[mm]$	**Weight [g]**	**Parallel jaw motion**	**Max. gripping force** $[\ mN]$	**Max. gripping stroke** $[\mu m]$	**Gripping range** $[\mu m]$	**Specific work**[0] $[J/kg]$
Described in this paper	$24.5 \times 3 \times 0.81$	0.1	Yes	575	268	100-368[2]	1.179
[31]	$15.5 \times 8.4 \times 0.5$[1]	0.158	Yes	178	800	-	< 0.901[4]
[31]	$15.5 \times 8.4 \times 0.5$[1]	0.164	Yes	125	240	-	< 0.183[4]
[27]	$40 \times 11 \times 0.6$ (one jaw)	2.1	No	203	1500	500-1500	0.145
[28]	$13 \times 1 \times 0.4$	0.2	No	80	160	0-160	0.064
[32]	$36 \times 16.5 \times 5$[1]	8.35[3]	Yes	1000	250	-	< 0.030[4]
[33]	$29.2 \times 20.91 \times -$[1]	-	No	159	515	100-1000	-
[18]	$50 \times 30 \times -$[1]	-	Yes	950	100	-	-

[0] The specific work is defined by the $stroke \times force/weight$.
[1] The devices listed show the dimensions and weights for the gripper mechanism only (i.e., not including the actuator).
[2] The gripping range could be increased by adding spacing layers between the two gripper parts.
[3] The weight has been estimated from the given dimensions.
[4] The specific work for these grippers does not include the piezoelectric actuator and therefore can not be compare with the gripper described in this paper.

$250\,\mu\mathrm{m}$ in thickness and approaching the weight of the robot. Significantly, we note that the gripper itself was able to hold a weight forty times its mass. Further, we are beginning to take advantage of the maneuverability of the robot to change a gripped object's position and orientation.

However, for the current experiments, objects were manually placed under the gripper of the robot. In the future, we plan to integrate a visual sensor and closed-loop locomotion control [10] to potentially improve the manipulation capability of the robot. We also aim to incorporate self-sensing [29] to detect when an object is grasped and modulate the gripping force for robust grasping.

Another consideration is energy storage. The gripper and the robot are driven by an external source of power which could limit their applications. A possible solution could be to use an untethered robot such as HAMR-F [30] which is fully autonomous and operates with similar voltages used in in this paper.

Finally, we hope to further scale down the gripper by using thinner piezoelectric materials to make it adaptable to smaller robots (e.g., the RoboBee [3]) and further increase the range of possible applications (e.g., milligram-scale clutches [13]).

Ultimately, we expect that the addition of such novel manipulation capabilities will greatly increase the effectiveness of these miniature robots for accomplishing real-world tasks.

ACKNOWLEDGEMENT

We thank Peter A. York and all other members of the Harvard Microrobotics Laboratory for invaluable support and discussions.

REFERENCES

[1] K. Jayaram and R. J. Full, "Cockroaches traverse crevices, crawl rapidly in confined spaces, and inspire a soft, legged robot," *Proceedings of the National Academy of Sciences*, vol. 113, no. 8, pp. E950–E957, 2016.

[2] O. Khatib, "Mobile manipulation: The robotic assistant," *Robotics and Autonomous Systems*, vol. 26, no. 2-3, pp. 175–183, 1999.

[3] N. T. Jafferis, E. F. Helbling, M. Karpelson, and R. J. Wood, "Untethered flight of an insect-sized flapping-wing microscale aerial vehicle," *Nature*, vol. 570, no. 7762, p. 491, 2019.

[4] M. Graule, P. Chirarattananon, S. Fuller, N. Jafferis, K. Ma, M. Spenko, R. Kornbluh, and R. Wood, "Perching and takeoff of a robotic insect on overhangs using switchable electrostatic adhesion," *Science*, vol. 352, no. 6288, pp. 978–982, 2016.

[5] Y. Chen, H. Wang, E. F. Helbling, N. T. Jafferis, R. Zufferey, A. Ong, K. Ma, N. Gravish, P. Chirarattananon, M. Kovac, *et al.*, "A biologically inspired, flapping-wing, hybrid aerial-aquatic microrobot," *Science Robotics*, vol. 2, no. 11, p. eaao5619, 2017.

[6] S. de Rivaz, B. Goldberg, N. Doshi, K. Jayaram, J. Zhou, and R. J. Wood, "Inverted and vertical climbing of a quadrupedal microrobot using electroadhesion," *Science Robotics*, vol. 3, no. 25, 2018.

[7] N. Doshi, K. Jayaram, B. Goldberg, Z. Manchester, R. J. Wood, and S. Kuindersma, "Contact-implicit optimization of locomotion trajectories for a quadrupedal microrobot," in *2018 Robotics Science and Systems*, 2018, in review.

[8] Y. Chen, N. Doshi, B. Goldberg, H. Wang, and R. J. Wood, "Controllable water surface to underwater transition through electrowetting in a hybrid terrestrial-aquatic microrobot," *Nature Communications*, vol. 9, no. 1, p. 2495, June 2018.

[9] R. St. Pierre and S. Bergbreiter, "Toward autonomy in sub-gram terrestrial robots," *Annual Review of Control, Robotics, and Autonomous Systems*, vol. 2, pp. 231–252, 2019.

[10] N. Doshi, K. Jayaram, S. Castellanos, S. Kuindersma, and R. J. Wood, "Effective locomotion at multiple stride frequencies using proprioceptive feedback on a legged microrobot," *Bioinspiration & biomimetics*, 2019.

[11] W. Driesen, T. Varidel, S. Régnier, and J.-M. Breguet, "Micro manipulation by adhesion with two collaborating mobile micro robots," *Journal of micromechanics and microengineering*, vol. 15, no. 10, p. S259, 2005.

[12] R. O. Ambrose, R. T. Savely, S. M. Goza, P. Strawser, M. A. Diftler, I. Spain, and N. Radford, "Mobile manipulation using nasa's robonaut," in *IEEE International Conference on Robotics and Automation, 2004. Proceedings. ICRA'04. 2004*, vol. 2. IEEE, 2004, pp. 2104–2109.

[13] Y. Peng, Y. Peng, X. Gu, J. Wang, and H. Yu, "A review of long range piezoelectric motors using frequency leveraged method," *Sensors and Actuators A: Physical*, vol. 235, pp. 240 – 255, 2015. [Online]. Available: http://www.sciencedirect.com/science/article/pii/S0924424715301771

[14] B. Goldberg, N. Doshi, K. Jayaram, and R. J. Wood, "Gait studies for a quadrupedal microrobot reveal contrasting running templates in two frequency regimes," *Bioinspiration and Biomimetics*, vol. 12, no. 4, p. 046005, 2017.

[15] M. Savia and H. N. Koivo, "Contact micromanipulation—survey of strategies," *IEEE/ASME Transactions on Mechatronics*, vol. 14, no. 4, pp. 504–514, 2009.

[16] J. Cecil, M. B. R. Kumar, Y. Lu, and V. Basallali, "A review of micro-devices assembly techniques and technology," *The International Journal of Advanced Manufacturing Technology*, vol. 83, no. 9-12, pp. 1569–1581, 2016.

[17] A. Nikoobin and M. H. Niaki, "Deriving and analyzing the effective parameters in microgrippers performance," *Scientia Iranica*, vol. 19, no. 6, pp. 1554 – 1563, 2012. [Online]. Available: http://www.sciencedirect.com/science/article/pii/S1026309812002313

[18] M. N. M. Zubir, B. Shirinzadeh, and Y. Tian, "A new design of piezoelectric driven compliant-based microgripper for micromanipulation," *Mechanism and Machine Theory*, vol. 44, no. 12, pp. 2248 – 2264, 2009. [Online]. Available: http://www.sciencedirect.com/science/article/pii/S0094114X09001359

[19] K. Jayaram, J. Shum, S. Castellanos, E. F. Helbling, and R. J. Wood, "Scaling down an insect-size microrobot, hamr-vi into hamr-jr," in *2020 IEEE International Conference on Robotics and Automation (ICRA)*. IEEE, 2020.

[20] J. D. Ervin and D. Brei, "Recurve piezoelectric-strain-amplifying actuator architecture," *IEEE/ASME Transactions on Mechatronics*, vol. 3, no. 4, pp. 293–301, 12 1998.

[21] O. Seresta, S. Ragon, M. Abdalla, G. rdal, and D. Lindner, "Design of a recurve actuator for maximum energy efficiency," *Smart Materials and Structures, 15 (6)*, vol. 15, 12 2006.

[22] J. D. Ervin and D. E. Brei, "Parallel and serial connections for piezoceramic recurve actuator arrays," in *Smart Structures and Materials 1998: Mathematics and Control in Smart Structures*, V. V. Varadan, Ed., vol. 3323, International Society for Optics and Photonics. SPIE, 1998, pp. 732 – 742. [Online]. Available: https://doi.org/10.1117/12.316352

[23] R. O. Ritchie, "Mechanisms of fatigue-crack propagation in ductile and brittle solids," *International Journal of Fracture*, vol. 100, pp. 55–83, 1999.

[24] N. T. Jafferis, M. J. Smith, and R. J. Wood, "Design and manufacturing rules for maximizing the performance of polycrystalline piezoelectric bending actuators," *Smart Materials and Structures*, vol. 24, no. 6, p. 065023, 2015. [Online]. Available: http://stacks.iop.org/0964-1726/24/i=6/a=065023

[25] E. F. Crawley and E. H. Anderson, "Detailed models of piezoceramic actuation of beams," 1989.

[26] N. Doshi, B. Goldberg, R. Sahai, N. Jafferis, D. Aukes, and R. J. Wood, "Model driven design for flexure-based microrobots," in *2015 IEEE/RSJ International Conference on Intelligent Robots and Systems (IROS)*, Sept 2015, pp. 4119–4126.

[27] R. K. Jain, S. Majumder, B. Ghosh, and S. Saha, "Design and manufacturing of mobile micro manipulation system with a compliant piezoelectric actuator based micro gripper," *Journal of Manufacturing Systems*, vol. 35, pp. 76 – 91, 2015. [Online]. Available: http://www.sciencedirect.com/science/article/pii/S0278612514001472

[28] J. Agnus, P. De Lit, C. Clevy, and N. Chaillet, "Description and performances of a four-degrees-of-freedom piezoelectric gripper," in *Proceedings of the IEEE International Symposium onAssembly and Task Planning, 2003.*, July 2003, pp. 66–71.

[29] K. Jayaram, N. Jafferis, N. Doshi, B. Goldberg, and R. J. Wood, "Concomitant sensing and actuation for piezoelectric microrobots," *Smart Materials and Structures*, 2018, in review.

[30] B. Goldberg, R. Zufferey, N. Doshi, E. F. Helbling, G. Whittredge, M. Kovac, and R. J. Wood, "Power and control autonomy for high-speed locomotion with an insect-scale legged robot," *IEEE Robotics and Automation Letters*, vol. 3, no. 2, pp. 987–993, 2018.

[31] A. Menciassi, A. Eisinberg, M. Mazzoni, and P. Dario, "A sensorized /spl mu/electro discharge machined superelastic alloy microgripper for micromanipulation: simulation and characterization," in *IEEE/RSJ International Conference on Intelligent Robots and Systems*, vol. 2, Sep. 2002, pp. 1591–1595 vol.2.

[32] M. Goldfarb and N. Celanovic, "Flexure-based gripper for small-scale manipulation," *Robotica*, vol. 17, pp. 181 – 187, 03 1999.

[33] K. Jayaram and S. Joshi, "Development of a flexure-based, force-sensing microgripper for micro-object manipulation," *Journal of Micromechanics and Microengineering - J MICROMECHANIC MICROENGINEER*, vol. 20, 01 2010.